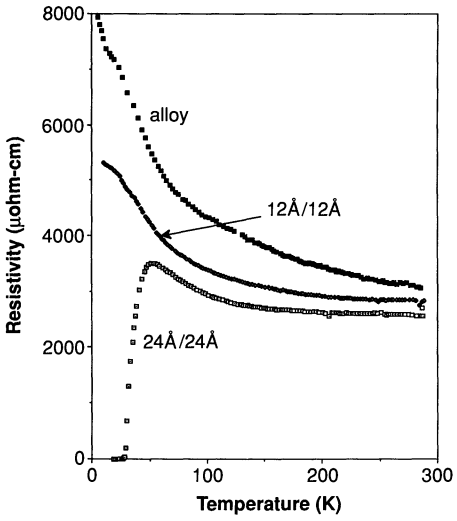

Fig. 5. Resistivity versus temperature curves for a $Y_{0.5}Pr_{0.5}BCO$ alloy *a*-axis film, and for 12 Å/12 Å *a*-axis, and a 24 Å/24 Å *a*-axis YBCO/PBCO superlattices.

the same CuO_2 planes are superconducting or insulating in narrow strips depending whether the rows of atoms in the neighboring rare earth plane are Y or Pr.

Lastly, we mention that in a 12 Å/12 Å *a*-axis superlattice, the system should have quasi-1D behavior, if as seems likely the CuO_2 planes are weakly coupled to each other so that pure YBCO itself is intrinsically close to a 2D system (*14*). When the YBCO layers are very thin and the PBCO layers thick enough so as to obtain a decoupling in the vertical direction the current will flow thru *b*-axis threads with a cross section of ~4 Å by ~d_s (d_s is the YBCO layer thickness) since the conduction in *a*-axis films is predominantly along the *b*-axis. Hence, there is some length scale of *a*-axis modulation where crossover occurs from quasi-2D to quasi-1D behavior. This transition should occur when the YBCO thickness is less than ξ_{ab} = 10 to 20 Å. Finally, for thicker YBCO layers, and as the temperature is decreased below T_c and the superconducting coherence length decreases, a crossover from 1D to 2D is expected at a temperature T^* at which ξ_{ab} becomes less than the YBCO thickness.

REFERENCES AND NOTES

1. U. Poppe *et al.*, *Solid State Commun.* **71**, 569 (1989).
2. J.-M. Triscone, M. G. Karkut, L. Antognazza, O. Brunner, Ø. Fischer, *Phys. Rev. Lett.* **63**, 1016 (1989).
3. J.-M. Triscone *et al.*, *ibid.* **64**, 804 (1990).
4. Q. Li *et al.*, *ibid.*, p. 3086.
5. D. H. Lowndes *et al.*, *ibid.* **65**, 1160 (1990).
6. C. B. Eom, A. F. Marshall, S. S. Laderman, R. D. Jacowitz, T. H. Geballe, *Science* **249**, 1549 (1990).
7. C. B. Eom *et al.*, *Appl. Phys. Lett.* **55**, 595 (1989).
8. C. B. Eom *et al.*, *Physica C* **171**, 351 (1990).
9. A. Inam *et al.*, *Appl. Phys. Lett.* **57**, 2484 (1990).
10. N. G. Stoffel, P. A. Morris, W. A. Bonner, B. J. Wilkens, *Phys. Rev. B* **37**, 2297 (1988).
11. Some samples had higher resistivities that the one presented on Fig. 5 which could be due to differences in grain size or in grain boundaries in these particular films.
12. The T_c in the (YPr)BCO alloys is very sensitive to small composition changes in the region of 50% Pr, that is probably the reason why in our case we find the *a*-axis 50/50 alloy not superconducting. A T_{co} of 12 K has been reported for the *c*-axis 50/50 alloy by J.-M. Triscone *et al.* (*3*).
13. S. J. Rothman *et al.*, paper presented at the 1989 TMS Fall Meeting Symposium on Atomic Migration and Defects in Materials.
14. M. Tachiki and S. Takahashi, *Solid State Commun.* **70**, 291 (1989).

15. This work has been supported by AFOSR under contract F49620-88-004, by the Center for Research in Superconductivity and Superconducting Electronics under contract F49620-88-C-001, and by the Stanford Center for Materials Research under the NSFMRL program.

29 October 1990; accepted 20 December 1990

Determination of Membrane Protein Structure by Rotational Resonance NMR: Bacteriorhodopsin

F. CREUZET,* A. MCDERMOTT,† R. GEBHARD, K. VAN DER HOEF, M. B. SPIJKER-ASSINK, J. HERZFELD, J. LUGTENBURG, M. H. LEVITT,‡ R. G. GRIFFIN

Rotationally resonant magnetization exchange, a new nuclear magnetic resonance (NMR) technique for measuring internuclear distances between like spins in solids, was used to determine the distance between the C-8 and C-18 carbons of retinal in two model compounds and in the membrane protein bacteriorhodopsin. Magnetization transfer between inequivalent spins with an isotropic shift separation, δ, is driven by magic angle spinning at a speed ω_r that matches the rotational resonance condition $\delta = n\omega_r$, where *n* is a small integer. The distances measured in this way for both the 6-s-*cis*- and 6-s-*trans*-retinoic acid model compounds agreed well with crystallographically known distances. In bacteriorhodopsin the exchange trajectory between C-8 and C-18 was in good agreement with the internuclear distance for a 6-s-*trans* configuration [4.2 angstroms (Å)] and inconsistent with that for a 6-s-*cis* configuration (3.1 Å). The results illustrate that rotational resonance can be used for structural studies in membrane proteins and in other situations where diffraction and solution NMR techniques yield limited information.

MANY QUESTIONS CONCERNING the structure and function of proteins can be answered with a technique that provides information on a few internuclear distances. For example, the conformations of prosthetic groups or key functional intermediates may often be specified by measurement of a few through-space distances. This realization originally stimulated the development of ^1H solution NMR experiments, which use nuclear Overhauser effect (NOE) difference spectra to estimate distances in proteins and nuclei acids (*1*). Initially, NOE studies were focused on small parts of the macromolecule, but in the past few years, two-dimensional (2D) and 3D NOE experiments have become commonplace, resulting in complete 3D solution structures of proteins and nucleic acids (*2, 3*).

For a number of reasons, 2D and 3D solution experiments are limited to relatively small proteins (≲20 kD). Thus, structural data on large proteins, membrane proteins, self-assembling proteins, or insoluble proteins are generally not accessible with this approach. Nevertheless, it is still possible to address a variety of structural questions in these systems with high-resolution solid-state NMR techniques, such as magic angle spinning (MAS) (*3–6*). These methods were originally developed to enhance resolution by attenuation of dipolar couplings and other anisotropic interactions (*7, 8*). However, structural information is contained in the dipolar couplings, and several techniques have been described that reintroduce this information selectively without sacrificing sensitivity and resolution. One recent and generally applicable approach for measuring homonuclear distances is based on rotational resonance in isolated spin pairs

F. Creuzet, A. McDermott, M. H. Levitt, Francis Bitter National Magnet Laboratory, Massachusetts Institute of Technology, Cambridge, MA 02139.
R. Gebhard, K. van der Hoef, M. B. Spijker-Assink, J. Lugtenburg, Gorlaeus Laboratorium, Rijksuniversiteit te Leiden, NL-2300 RA Leiden, The Netherlands.
J. Herzfeld, Department of Chemistry, Brandeis University, Waltham, MA 02254.
R. G. Griffin, Francis Bitter National Magnet Laboratory and Department of Chemistry, Massachusetts Institute of Technology, Cambridge, MA 02139.

*Present address: Unité Mixte de Recherche, CNRS/ Sainte Gobain, 39 Quai Lucien Lefranc, 93303 Aubervilliers Cedex, France.
†Present address: Department of Chemistry, Columbia University, New York, NY 10027.
‡Present address: Center in Superconductivity, University of Cambridge, Madingley Road, Cambridge CB3 0HE, United Kingdom.

(*9, 10*). Specifically, homonuclear pairs of spin-$^{1/2}$ nuclei such as ^{13}C-^{13}C (*11, 12*) or ^{31}P-^{31}P (*13*) are introduced into a lattice in a magnetically dilute fashion, and the spinning speed, ω_r, is adjusted to match a submultiple of the isotropic shift separation, δ. At this rotational resonance condition—$\delta = n\omega_r$, where n is a small integer—there is a partial and spectrally selective recoupling of the dipolar spin pair (*9, 10, 12, 14, 15*). Measurement of spin dynamics at rotational resonance therefore provides a means to determine internuclear distances (*11*).

The spectral behavior of an isolated homonuclear spin pair at rotational resonance has been described in detail experimentally (*11–13, 16*) and theoretically (*17, 18*) and is characterized by two important effects. First, when the internuclear coupling is large compared to the linewidths, as occurs for a small internuclear separation, and n is small, then the rotational resonance spectra exhibit line shapes with fine structure that depends on the internuclear distance and relative orientation of the chemical shift tensors. The second effect involves the exchange of Zeeman order between rotationally resonant spins. In this case, the Zeeman magnetization of one of the coupled spins is selectively inverted and the rotor-driven exchange of magnetization is followed in time. The trajectory of the difference Zeeman polarization $\langle I_z - S_z \rangle (t)$ may be simulated to yield the internuclear distance (*12, 17*). Unlike the line shape analysis, appreciable magnetization exchange effects are observed even when the dipolar couplings are comparable to or smaller than the linewidths. The dipolar couplings must only exceed the inverse of the spin lattice relaxation time, T_1^{-1}, which in solids may be of the order of seconds. Thus this exchange provides a means to sample weak couplings and therefore long internuclear distances. For ^{13}C-^{13}C spin pairs in small molecules (molecular mass of 100 to 300 daltons), it has been possible to measure distances up to 5.0 Å with an accuracy of better than 0.5 Å (*12, 16*). In this report we describe the extension of the technique to distance measurements in a membrane protein, bacteriorhodopsin (bR), with an effective molecular mass of ~35 kD.

Bacteriorhodopsin, the principal protein component of the outer membrane of *Halobacterium halobium*, where it serves as a light-driven proton pump. Although it apparently serves as an energy-transducing system for *H. halobium*, its architecture bears no similarity to the architecture of the more common photosynthetic enzymes; rather, bR belongs among the retinal-binding proteins, which more generally serve as sensory systems. Because of the protein environment of the chromophore, the absorption spectra of these pigments vary in a dramatic fashion and with an obvious pertinence to their functions. Much of the structural and spectroscopic work on bR has focused on delineating the factors that contribute to this wavelength regulation. In contrast to the situation for rhodopsin (*19, 20*), the NMR and vibrational spectra of retinal show dramatic structural changes upon binding to bR. One of the most significant of these changes is the isomerization about the 6–7 bond. This isomerization extends the polyene chain and may therefore be expected to contribute a substantial fraction of the red shift of the pigment upon binding (*21*). In retinoid compounds, both a 6-s-*cis* and a 6-s-*trans* form are possible and are predicted to be comparable energetically (*22*). Chemical shift data of the 5-^{13}C indicate that the conformation changes from a 6-s-*cis* form observed in solution to a 6-s-*trans* form in bR (*23, 24*). However, since this interpretation of the chemical shift data has been questioned (*25*), we have been interested in developing an unambiguous method for determining the conformation of retinal in this pigment.

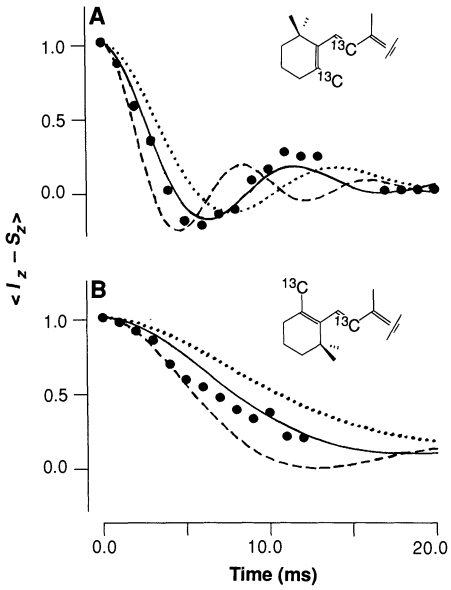

Fig. 1. (**A**) Magnetization transfer data (filled circles) at 25°C for the $n = 1$ rotational resonance of 6-s-*cis* [8,18,-$^{13}C_2$]retinoic acid, along with calculated curves for three distances: 2.7 Å (lower dashed line); 3.0 (solid line); and 3.3 Å (upper dashed line). The inset shows the geometry of the ring-polyene linkage for this crystallographic form. The abscissa values were generated by measuring the centerband intensities for both sites, normalizing the intensities to the zero mixing time values and taking the difference. Curves were calculated as described elsewhere (*17*). (**B**) Magnetization transfer data (filled circles) at 25°C for the $n = 1$ rotational resonance of 6-s-*trans* [8-18-$^{13}C_2$]retinoic acid, along with calculated curves for three distances: 3.7 Å (lower dashed line); 4.1 Å (solid line); and 4.4 Å (upper dashed line). The inset shows the geometry of the ring-polyene linkage for this crystallographic form.

To address the question of the configuration about the 6–7 bond, we have regenerated bR with a double ^{13}C-labeled [8,18-$^{13}C_2$]retinal. The distance between carbons C-8 and C-18 is quite different in the 6-s-*cis* (~3.1 Å) and the 6-s-*trans* (~4.2 Å) forms (*26, 27*). Our approach has been to measure the rotationally driven Zeeman exchange curves for the doubly labeled retinal bound to bR, as well as for two structural analogs for which crystal structures have been solved: the monoclinic form of retinoic acid, which is characterized by a planar 6-s-*trans* configuration, and the triclinic form, which is 6-s-*cis* with the β-ionone ring rotated ~35° out of the plane of the polyene chain (*26*).

The NMR experiment consists of preparing enhanced ^{13}C magnetization by cross-polarization from the ^1H spin reservoir, storing it along the z-axis of the rotating frame, and then selectively inverting the magnetization at one site. Following a mixing period of duration τ, during which rotor-driven magnetization exchange takes place, the remaining z-magnetization is sampled by an additional 90° pulse (*11*). In the absence of significant spin-lattice relaxation during τ, the exchange process is characterized by the decay curve for the difference magnetization $\langle I_z - S_z \rangle (\tau)$ (*28*).

For the model compound experiments, [8,18-$^{13}C_2$]retinoic acid was isotopically diluted with a fivefold excess of natural abundance retinoic acid, in order to ensure that the spin pairs were magnetically dilute, and crystallized according to previously described procedures (*24*). In the 6-s-*cis* retinoic acid, the internuclear distance between the C-8 and the C-18 is 3.1 Å, resulting in a dipolar coupling of 255 Hz. Correspondingly, the [8,18-$^{13}C_2$]compound exhibits a rapid transfer of magnetization, on the time scale of a few milliseconds at rotational resonance. Figure 1A shows the measured and calculated magnetization transfer curves for the $n = 1$ condition for this system, and the oscillatory behavior observed experimentally is in good agreement with the theoretical prediction. For the $n = 1$ data shown in Fig. 1, the decay profile is rather insensitive to errors in the tensor orientations or anisotropy parameters but is quite sensitive to the distance (*26*). The best fit is obtained for 3.0 Å, in good agreement with the crystallographic determination. In the 6-s-*trans* form of retinoic acid, the internuclear distance between C-8 and C-18 nuclei is ~4.2 Å, with a dipolar coupling of 103 Hz (Fig. 1B); thus, the time scale of the magnetization decay is noticeably slower than for the triclinic form. Again, however, we find good agreement between measure-

ment and calculation for the $n = 1$ resonance condition.

The simulation of these exchange curves was accomplished by using a procedure described previously (*17*). We used chemical shift tensor values extracted from a low spinning speed spectrum (~2.5 kHz) with a Herzfeld-Berger analysis (*29*) and the zero-quantum T_2 value (T_2^{ZQ}) estimated from the sum of the individual line widths after correcting for magnet inhomogeneity. This method for determining T_2^{ZQ} assumes uncorrelated fields for the two sites (*30*) and has been shown to be valid for two cases in which two ^{13}C atoms are separated by distances smaller than those considered here; thus we assumed it to be correct for the ^{13}C atoms in retinal and in bR. The tensor orientations were derived from the crystal structure of retinoic acid, together with the single-crystal data for a C=C moiety, which indicate that the most shielded tensor element is perpendicular to the polyene plane and the intermediate element lies along the double bond (*31, 32*), while for C-18 the most shielded element lies along the C–C bond (*32*).

The measurement of magnetization exchange for [8,18-$^{13}C_2$]retinal-bR, as well as its interpretation, differed in significant respects from that of the retinoic acids. Most notably, because of its large molecular weight, bR exhibits a substantial natural abundance ^{13}C background signal that is relatively featureless because of contributions from many different carbon species. We removed this signal from that of the 8-^{13}C and 18-^{13}C specifically labeled sites by subtraction of an identically prepared spectrum of an unlabeled bR sample. In Fig. 2, spectra are shown for both the [8,18-$^{13}C_2$]retinal-bR and the natural abundance bR after selective inversion of the methyl region and no mixing period. Below these spectra is the difference spectrum, which shows only the contribution of the [8,18-$^{13}C_2$]retinal labels. In order to avoid any complications due to molecular motion, we acquired all of these spectra at −30°C.

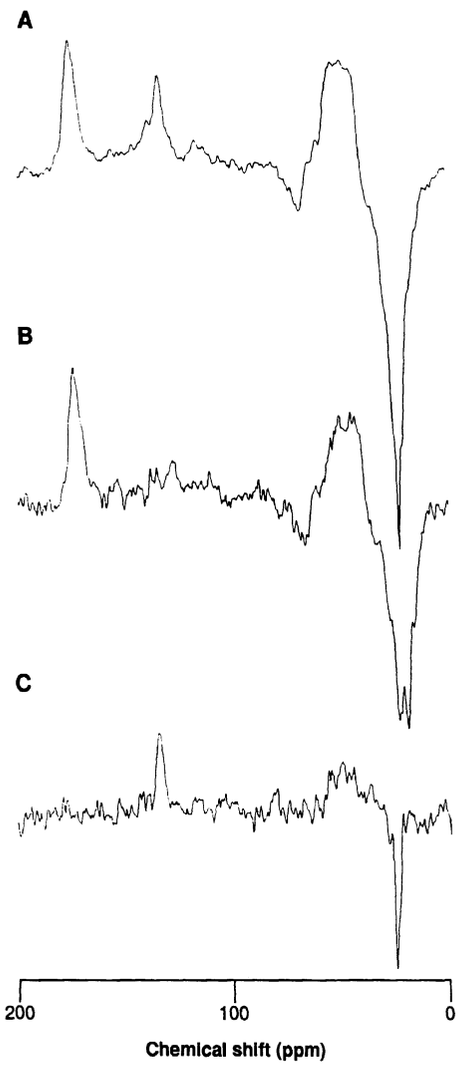

Fig. 2. (**A**) ^{13}C-MAS spectrum at −30°C of [8,18-$^{13}C_2$]retinal-bR following selective inversion of the methyl region of the spectrum; (**B**) the ^{13}C spectrum of natural abundance bR following selective inversion of the methyl region, and (**C**) the difference between (A) and (B), yielding the spectrum of the labels alone. Intensities were taken from difference spectra, such as this one, to yield a magnetization transfer curve (Fig. 3).

The doubly labeled retinal residue in bR has broader lines than in retinoic acid (100 to 150 Hz for bR rather than 35 to 50 Hz for retinoic acid). This difference, which probably arises from a heterogeneity in chemical environments or from incomplete proton decoupling, results in a shorter T_2^{ZQ} for the protein as compared with the model systems, assuming uncorrelated random field relaxation. The rapid zero-quantum relaxation in turn leads to much slower magnetization exchange in bR.

The $n = 1$ magnetization transfer curve for the [8,18-$^{13}C_2$]retinal-bR, together with two simulations, is shown in Fig. 3. The lower calculated curve is based on the tensor and distance parameters used in the triclinic 6-s-*cis* form of retinoic acid (Fig. 1), but with the T_2^{ZQ} value as determined for bR, while the second curve involves the tensor and distance parameters for the monoclinic 6-s-*trans* form combined with the T_2^{ZQ} as determined for bR. There is good agreement with the distance for a 6-s-*trans* configuration and substantial disagreement for a 6-s-*cis* form.

Measurements of magnetization transfer at spinning speeds away from rotational resonance were also performed for both model compounds as well as for bR, and in all cases we found the transfer to be negligible on a 40-ms time scale. This control confirms that the origin of the magnetization transfer is a rotational resonance effect

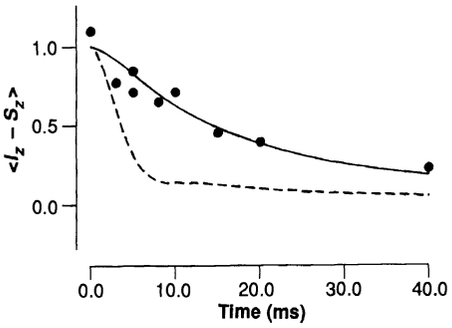

Fig. 3. Magnetization transfer data at −30°C measured for the [8,18-$^{13}C_2$]retinal-bR along with calculated curves based on the known distances and geometries for the 6-s-*cis* (dashed line) and the 6-s-*trans* (solid line) configurations, combined with the T_2^{ZQ} derived from the measured linewidths for the 8,18-$^{13}C_2$-retinal-bR. The data agree well with the 6-s-*trans* configuration and not with the 6-s-*cis* configuration.

arising from a dipolar coupling between the two sites. In addition, we do not observe a change in linewidth or line shape on rotational resonance for any of the systems considered here, an effect which is consistent with numerical simulations. This response may occur in many studies of macromolecules in which the dipolar couplings are comparable to the linewidth. Thus the coupling that is easily detectable in a magnetization transfer experiment may not be apparent in the linewidth experiment.

For a system with a short T_2^{ZQ} and weak dipolar couplings, the higher orders ($n > 1$) of rotational resonance may result in prohibitively slow magnetization transfer curves. In this report, we have focused attention on the $n = 1$ resonance for bR, since for the [8,18-$^{13}C_2$]retinal it is insensitive to the details of the chemical shielding tensor values and orientations. This curve alone adequately defines the through-space distance between C-8 and C-18. As discussed elsewhere (*16, 17*), the higher-order rotational resonances may be useful for defining relative tensor orientations once the bond length is known. It is also important to quantify error limits in the distance and the sensitivity of the measured distance to the various parameters, especially the tensor angles and the T_2^{ZQ}. These characterizations should be particularly useful for situations in which suitable model compounds for the spin pair in question are absent. However, judging from the analysis shown in this report, we can conclude unambiguously that the retinal in bR is in the 6-s-*trans* configuration. Other structural questions concerning bR and other biopolymers can be addressed with the rotational resonance technique.

REFERENCES AND NOTES

1. A. G. Redfield and R. K. Gupta, *Cold Spring Harbor Symp. Quant. Biol.* **36**, 405 (1971).

2. R. R. Ernst, G. Bodenhausen, A. Wokaun, *Principles of Nuclear Magnetic Resonance in One and Two Dimensions* (Oxford Univ. Press, Oxford, 1990).
3. K. Wüthrich, *NMR of Proteins and Nucleic Acids* (Wiley, New York, 1986).
4. R. G. Griffin *et al.*, in *Physics of NMR Spectroscopy in Biology and Medicine*, B. Maraviglia, Ed. (North-Holland, New York, 1988), pp. 203–266.
5. E. R. Andrew, A. Bradbury, R. G. Eades, *Nature* **182**, 1659 (1958).
6. I. J. Lowe, *Phys. Rev. Lett.* **2**, 285 (1959).
7. A. Pines, M. G. Gibby, J. S. Waugh, *J. Chem. Phys.* **59**, 569 (1973).
8. J. Schaefer and E. O. Stejskal, *J. Am. Chem. Soc.* **98**, 1031 (1976).
9. E. R. Andrew, S. Clough, L. F. Farnell, T. D. Gledhill, I. Roberts, *Phys. Lett.* **21**, 505 (1966).
10. E. R. Andrew, A. Bradbury, R. G. Eades, V. T. Wynn, *ibid.* **4**, 99 (1963).
11. D. P. Raleigh, M. H. Levitt, R. G. Griffin, *Chem. Phys. Lett.* **146**, 71 (1988).
12. D. P. Raleigh, F. Creuzet, S. K. Das Gupta, M. H. Levitt, R. G. Griffin, *J. Am. Chem. Soc.* **111**, 4502 (1989).
13. A. E. McDermott *et al.*, *Biochemistry* **29**, 5767 (1990).
14. M. G. Columbo, B. H. Meier, R. R. Ernst, *Chem. Phys. Lett.* **146**, 189 (1988).
15. E. W. J. R. Maas and W. S. Veeman, *ibid.* **149**, 170 (1988).
16. F. Creuzet, D. P. Raleigh, M. H. Levitt, R. G. Griffin, unpublished results.
17. M. H. Levitt, D. P. Raleigh, F. Creuzet, R. G. Griffin, *J. Chem. Phys.* **92**, 6347 (1990).
18. Z. Gan and D. M. Grant, *Mol. Phys.* **67**, 1419 (1990).
19. W. J. DeGrip, *Photochem. Photobiol.* **48**, 799 (1988).
20. R. A. Mathies, S. O. Smith, I. Palings, in *Biological Applications of Raman Spectroscopy*, T. Spiro, Ed. (Wiley, New York, 1987), pp. 59–108.
21. B. Honig, A. D. Greenburg, U. Dinur, T. G. Ebrey, *Biochemistry* **15**, 4593 (1976).
22. B. Honig, B. Hudson, B. D. Sykes, M. Karplus, *Proc. Natl. Acad. Sci. U.S.A.* **68**, 1289 (1971).
23. G. S. Harbison *et al.*, *Biochemistry* **24**, 6955 (1985).
24. G. S. Harbison *et al.*, *J. Am. Chem. Soc.* **107**, 4809 (1985).
25. H. Rodman-Gilson and B. Honig, *ibid.* **110**, 1943 (1988).
26. C. H. Stam and C. H. MacGillavry, *Acta Cryst. allogr.* **16**, 62 (1963).
27. C. H. Stam, *Acta Crystallogr. Sect. B* **28**, 2936 (1972).
28. This procedure differed from that used previously, in that here the centerband intensity was used, while in our previous analysis of Zn acetate and tyrosine ethyl ester the sum of the integrated centerband and sidebands was used. The major reason for this change in analysis was to improve the signal-to-noise ratio in the intensity measurement, since the signal-to-noise ratio for bR is such that the sidebands and the wings of the centerband cannot be measured accurately. We find that analysis of zinc acetate and retinoic acid data by this method (see below) results in good agreement with crystallographic distances. Furthermore, for the $n = 1$ resonance used here, the spinning speeds are large compared to $\Delta\sigma$ and therefore the sideband intensities, and the errors generated by ignoring them, are small.
29. J. Herzfeld and A. E. Berger, *J. Chem. Phys.* **73**, 6021 (1980).
30. A. Kubo and C. A. McDowell, *J. Chem. Soc. Faraday Trans.* **C84**, 3713 (1988).
31. E. K. Wolff, R. G. Griffin, J. S. Waugh, *J. Chem. Phys.* **67**, 2387 (1977).
32. M. Mehring, *Principles of High-Resolution NMR in Solids* (Springer-Verlag, Berlin, 1983), pp. 250–257.
33. Supported by the National Institutes of Health (GM-23403, GM-36810, GM-36920, and RR-00995), and by the Netherlands Foundation for Chemical Research and the Netherlands Organization for the Advancement of Scientific Research. F. C. was supported by a Bantrell Fellowship and A. M. by an American Cancer Society Postdoctoral Fellowship (PF-3283).

27 August 1990; accepted 9 November 1990

Baddeleyite-Type High-Pressure Phase of TiO_2

H. SATO, S. ENDO,* M. SUGIYAMA, T. KIKEGAWA, O. SHIMOMURA, K. KUSABA

A high-pressure phase of TiO_2, which had been observed by shock-wave experiments and remained unresolved, has been studied by in situ x-ray diffraction. The single phase was formed at 20 gigapascals and 770°C with the use of sintered-diamond multianvils; it has the same structure as baddeleyite, the stable phase of ZrO_2 at ambient conditions. The coordination number of Ti increases from six to seven across the rutile to baddeleyite transition, and the volume is reduced by approximately 9 percent.

STUDY OF PRESSURE-INDUCED PHASE transitions of dioxides provides an understanding of crystal structure and bonding and mineral stability in planets. The TiO_2 system provides an analog to the SiO_2 system; for example, stishovite (a high-pressure form of SiO_2) has a rutile structure. Many workers have investigated phase relations in the TiO_2 system (*1*). On the basis of shock-wave experiments, McQueen *et al.* (*2*) reported that TiO_2 underwent a phase transition beginning at 33 GPa and terminating at 100 GPa, accompanied by ~20% volume reduction. They found that the sample after compression to 75 GPa was a mixture of rutile and α-PbO_2 (columbite)–type structures. Mashimo *et al.* (*3*) observed a strong dependence of the onset pressure of the transition on the shock propagation direction. The transition began at 12.2, 17.0, or 33.7 GPa along the [100], [110], or [001] axis, respectively. These results were confirmed by Syono *et al.* (*4*), who reported, in addition, that this transition terminates at ~70 GPa and that another transition takes place around 100 PGa. These two transitions were not separately observed by either McQueen *et al.* (*2*) or Al'tshuler *et al.* (*5*).

The determination of the crystal structure of the phase beginning to appear at 12 to 34 GPa has been a problem for a quarter of a century. The α-PbO_2 phase in the sample recovered after compression beyond the transition pressure cannot be a candidate, because its volume is only ~2% smaller than that of rutile (*2*); the α-PbO_2 phase has been assumed to be a metastable modification of the high-pressure phase, which might have a structure such as that of fluorite. X-ray studies at room temperature have shown that no apparent phase transition occurs up to 18 GPa (*2*). However, in studies with a diamond-anvil cell and a laser heating technique, two different high-pressure phases were reported (*6*, *7*); one was a hexagonal phase with volume smaller by 10.5% than that of rutile at 25 GPa and room temperature after heating up to ~1000°C (*6*), and the other was an orthorhombic phase at 20 GPa after almost the same heat treatment (*7*). In this report we describe the in situ x-ray determination of the crystal structure of this high-pressure phase.

High pressure and high temperature were generated with so-called 6–8 type double-stage multianvils; sintered-diamond was used for the second-stage eight anvils (*8*). The synchrotron radiation used for the structure

H. Sato, S. Endo, M. Sugiyama, Research Center for Extreme Materials, Osaka University, Toyonaka, Osaka 560, Japan.
T. Kikegawa, National Laboratory for High Energy Physics, Tsukuba 305, Japan.
O. Shimomura, National Institute for Research in Inorganic Materials, Tsukuba 305, Japan.
K. Kusaba, Institute for Materials Research, Tohoku University, Sendai 980, Japan.

*To whom correspondence should be addressed.

Table 1. Observed (obs) and calculated (calc) x-ray diffraction data of TiO_2 at 20.3 GPa and room temperature. The sample was heated at 770°C for 30 min and then quenched to room temperature while at 20.3 GPa. Monoclinic cell parameters were determined to be $a = 4.64 \pm 0.01$ Å, $b = 4.76 \pm 0.01$ Å, $c = 4.81 \pm 0.01$ Å, $\beta = 99.2 \pm 0.4°$, $Z = 4$, and $V = 104.8 \pm 0.5$ Å^3 by the least-square method.

d_{obs} (Å)	Baddeleyite type			
	d_{calc} (Å)	h	k	l
3.37	3.36	0	1	1
3.32	3.30	1	1	0
2.858	2.869	1	1	$\bar{1}$
2.588	2.574	1	1	1
2.357	2.378	0	2	0
	2.376	0	0	2
2.281	2.289	2	0	0
1.987	2.000	2	1	$\bar{1}$
	1.984	1	2	$\bar{1}$
	1.982	1	0	2
1.834	1.830	1	1	2
1.803	1.799	2	0	$\bar{2}$
1.691	1.681	0	2	2
1.660	1.649	2	2	0
	1.639	1	2	$\bar{2}$
1.629	1.617	2	2	$\bar{1}$
1.532	1.526	3	0	0
1.494	1.503	0	1	3
	1.498	1	3	0
	1.497	1	1	$\bar{3}$
1.440	1.453	3	1	$\bar{1}$
	1.451	1	3	$\bar{1}$
	1.435	2	2	$\bar{2}$